Plant alkali content and radio wave communication efficiency in high intensity savanna wildfires

Kgakgamatso Marvel Mphale*, Malcom L. Heron

Department of Physics, University of Botswana, Plot 538 Ext. No. 4, Gaborone, Botswana

Received 9 December 2005; received in revised form 3 October 2006; accepted 20 October 2006
Available online 8 January 2007

Abstract

The flames of wildfires are weakly ionized gas. The ionization is mainly due to omnipresent alkali and alkaline earth metal species that are emitted from thermally decomposing plant structure into the flame during a wildfire. The amount of ionization in flames with alkali impurities is a factor of both the temperature and the quantity of the emitted alkali species in vegetation. Assuming a Maxwellian velocity distribution of flame particles and collision frequencies much higher than plasma frequencies, the propagation of radio waves through wildfires is predicted to have attenuation and phase shift. A theoretical model has been developed to predict propagation characteristics of HF–VHF radio signals at normal incidence to a high intensity wildfire fuel–flame interface. At the interface, the flame medium is modelled by a series of mini-slabs, each with a different but fixed electron density and dielectric permittivity governed by the Rayleigh distribution of temperature. Electron density in each mini-slab is calculated from thermal ionization of alkali species assuming the existence of thermal equilibrium. The model predicts average electron densities ranging from 10^{14} to $10^{17}\,m^{-3}$ for fuel–flame interfaces with maximum temperatures from 900 to 1200 K. Specific attenuation and phase shift for propagation in the ionized gas are calculated from the predicted average electron density and collision frequency. At collision frequency of $10^{11}\,s^{-1}$, radio signal specific attenuation for the simulated grassfires range from 0.001 to 0.49 dB m^{-1} while specific phase shift ranged from 0.0002 to 152° m^{-1} for the maximum temperature range of 900–1150 K.

Keywords: Radiowave; Wildfire; Attenuation; Thermal ionization; Grassfire; Savanna

1. Introduction

Tropical savannas are constantly threatened by frequent occurrence of wildfires, e.g., almost half of the northern Australia's savannas burn annually or biennially (Williams et al., 1999). Most of the fires occur during dry season when there are high fuel loads, which can be up to 13 tha^{-1}. Fires that occur during the season are often extensive and intense with flame temperatures in the range of 600–900 °C (Cheney et al., 1993; Clark et al., 2003).

During a wildfire, the organic structure of vegetation thermally crumbles to release omnipresent alkali and alkaline earth metal (AAEM) based nutrients, which are then convectively drawn into the combustion zone of the diffusion flames. Potassium species form a large fraction of the emissions (Westberg et al., 2003). Up to 28% of inherent potassium in plants is volatilized at combustion efficiency of 98% (Raison et al., 1985). The hot environment in the fire thermally

*Corresponding author. Tel.: +2673552137.
E-mail address: Mphalekm@mopipi.ub.bw (K.M. Mphale).

Nomenclature

$\vec{B}$	magnetic field
B_e	rotational constant
c	speed of light in vacuum $= 3 \times 10^8\ \mathrm{m\,s^{-1}}$
$\vec{E}$	electric field
E_d	dissociation energy (eV)
E_i	ionization energy (eV)
E_n	energy level (eV)
$G^0(T)$	Gibb's free energy temperature T
h	Planck's constant $= 6.626 \times 10^{-34}\ \mathrm{J\,s}$
$H^0(0)$	enthalpy for a particle formation at 0 K
K_B	Boltzmann's constant $= 8.617 \times 10^{-5}\ \mathrm{eV\,K^{-1}}$
K_I	ionization equilibrium constant
m	mass of an electron $= 9.11 \times 10^{-31}\ \mathrm{kg}$
m_A, m_B, m_{AB}	molar masses for particles A, B and AB
M_p	mass of potassium in flame per unit volume ($\mathrm{kg\,m^{-3}}$)
N_a	Avogadro's constant $= 6.022 \times 10^{23}$ atoms/mol
N_A, N_B, N_{AB}	number densities for particles A, B and AB ($\mathrm{m^{-3}}$)
N_e	electron density ($\mathrm{m^{-3}}$)
N_m, N_{m+}	number density for neutral and singly ionized particle ($\mathrm{m^{-3}}$)
N_n	number density of neutral flame gas ($\mathrm{m^{-3}}$)
N_p	total number of ionized potassium atoms ($\mathrm{m^{-3}}$)
P	total ionized gas pressure ($\mathrm{N\,m^{-2}}$)
P_k	percentage of potassium in volatiles
q_e	electron charge $= 1.602 \times 10^{-19}\ \mathrm{C}$
$Q_{A\,int}, Q_{B\,int}, Q_{AB\,int}$	internal partition functions for particles A, B and AB
Q_{m+}	internal partition function for singly ionized alkali
Q_m	internal partition function for an unionized alkali atom
T	flame temperature (K)
$\dot{x}$	drift velocity of average electron ($\mathrm{m\,s^{-1}}$)
$\ddot{x}$	average electron acceleration ($\mathrm{m\,s^{-2}}$)
V_f	volatile flux ($\mathrm{kg\,m^{-2}\,s^{-1}}$)
V_v	vertical velocity of volatie ($\mathrm{m\,s^{-1}}$)
V_v	vertical velocity of volatile ($\mathrm{m\,s^{-1}}$)

Greek symbols

α_f	flame attenuation constant
β	phase shift coefficient
γ	propagation constant
υ_{eff}	effective collision frequency
ω	propagation frequency
ω_n	statistical weights
ω_p	plasma frequency
η	potassium atoms in the flux per unit volume ($\mathrm{m^{-3}}$)
σ	electrical conductivity
σ_c	symmetry number

dissociates the AAEM species into atoms, which consequently ionize to give ions and electrons. Most of potassium species have low dissociation energies (e.g. 3.79 eV for K_2CO_3), therefore there are likely to produce most ionization when considering the low ionization potential of 4.34 eV for the element. Vodacek et al. (2002) estimate that 10–20% of potassium in vegetation is thermally ionized in wildfires. This makes wildfires a weakly ionized environment.

Particles in the weakly ionized medium collide with each other. Electron–neutral collision is the dominant form of particle interaction. The reason for the insignificance of other forms of interactions such as; electron–ion, electron–electron, ion–neutral, etc., is that; (a) compared to electrons, other particles are far much heavier and therefore less mobile and (b) electrons and ionized particles are less numerous than the neutrals. When the weakly ionized gas is illuminated with electromagnetic energy, electrons are accelerated by the electric field of the incident electromagnetic waves. Assuming that interaction between electrons and neutrals is elastic, the neutrals gain little kinetic energy during collisions mainly because they are relatively massive. Electrons are scattered isotropically but the average velocity after collision is zero. In this way energy is transferred from the electromagnetic wave to the neutral gas.

There have been anecdotal reports of failure to maintain radio communication at HF to UHF during wildfire suppression (Williams et al., 1970; Foster, 1976). This is a safety concern for fire fighters at fire grounds. Radio communication at fire grounds needs to be maintained at all times as it is a means by which fire fighters can be warned of an

impeding danger, e.g. of entrapment. Besides, fire fighters need to be continually updated on the fire behaviour conditions and communicate with each other or incident commander on best tactics for suppressing the threat. VHF/UHF mobile radios are used extensively for this purpose.

This paper numerically investigates the effect of temperature and potassium content on propagation characteristics of a narrow beam radio wave signal at fuel–flame interface (combustion zone) of annual *Sorghum* spp. grassfire. At the fuel–flame interface, the flame is divided into mini-slabs each having an average temperature governed by a Raleigh profile. The average temperature in each mini-slab is then used to determine electron density assuming thermal equilibrium. It also discusses possible scenarios that could cause radio communication blackout.

2. Theory

2.1. Vegetation combustion

An empirical formula of cellulose is often used to describe the combustion of dry plant matter, e.g., in Nussbaumer (2003) and Brown and Davis (1973). Nussbaumer has given a detailed description of combustion of plant matter that emphasizes on the importance of the availability of air. Nussbaumer described combustion to proceed as follows:

$$\begin{aligned} &CH_{1.44}O_{0.66} + 1.03\beta(O_2 + 3.76N_2) \\ &\quad \Rightarrow \text{Intermediates}(C, C_XH_Y, CO_2, H_2, CO, \text{etc.}) \\ &\quad \Rightarrow CO_2 + 0.72H_2O + (\beta - 1)O_2 + 3.87\beta N_2. \end{aligned} \quad (1)$$

The equation defines β as excess air ratio. Excess air ratio compares the amount of locally available combustion air to the stoichemetric amount. β is greater than unity for when local combustion air is in excess of the stoichemetric amount, otherwise is less than unity. Intermediate products, also termed pyrolysates are formed when a fuel undergoes thermal decomposition usually in an area of insufficient air (i.e., in a region where $\beta<1$). The pyrolysates are volatile and readily combust when they mix with oxygen of the air in the presence of a spark. During a grassfire, pyrolysates are drawn into the combustion zone where they are oxidized to produce water (H_2O) and carbon dioxide (CO_2) in an exothermic reaction. Not all pyrolysates enter the combustion zone; some escape the oxidation to be pollutants in the atmospheric air.

2.2. Alkali and alkaline earth metal contamination in plants

AAEMs, chlorine (Cl) and sulphur (S) are part of the inorganic ash material in a plant, which account for up to 10% of its dry weight. Plants require large quantities of these elements for a healthy growth. Consequently, the inorganics exist in substantial amount in cell fluids in vacuoles (Obernberger et al., 1997; Maser et al., 2002). Plant matter can contain up to 3.4% of the element potassium (K) (Radojevic, 2003). Savanna grasses such as *Sorghum* spp. in northern Australian tropical savanna contain; 0.22–1.50% K, 0.16–0.62% Ca, 0.01–0.12% Na and 0.10–0.64% Mg on dry weight basis (Cook and Andrew, 1991). In vegetation, AAEMs exist in different physical forms. They can exist; ionically or organically attached to oxygen-containing functional groups of the organic structure of the plants, as discrete particles in voids of the organic matrix and in solution form such as in xylem vessels.

2.3. Ionization in grassfires

2.3.1. Thermal ionization of flame species

The AAEM species are liberated when the organic structure of plants thermally decomposes (Westberg et al., 2003; Jensen et al., 2000; Olsson et al., 1997; Davidsson et al., 2002). This can occur at temperatures as low as 400 °C (Korsgren et al., 1999). During vegetation combustion, volatile K and Na species diffuse and attach to oxygen containing carboxyl groups in charcoal matrix forming organo-alkali structures such as K–O–C (see Okuno et al., 2005). Heating rates in wildfires are as high as 100 °C s^{-1} (Engstrom et al., 2004). The high combustion rates combined with forced gas convection of light gases such as hydrogen radical (H^+) through the organic structure facilitate rapid evolution of alkali atoms from the thermally decomposing charcoal into the grassfire flame. This occurs when H^+ and other light volatiles react with the alkali containing carboxyl groups to displace alkali atoms from charcoal attachment sites (Okuno et al., 2005). K and Na have low ionization potentials of 4.34 and 5.14 eV, respectively. At normal forest fire temperatures, Vodacek et al. (2002) have estimated that about 10–20% of K in vegetation is ionized.

High temperatures produced in the reaction zone of grassfire thermally excite flame component particles. The excited particles are then ionized to

produce electrons and ions on selective basis determined by temperature and ionization potential. Possible grassfire flame particles that could be appreciably thermally ionized are alkalis (e.g. K and Na), nitrogen monoxide (NO) and graphitic carbon (C_n). Combusting gases temperatures in grassland fires are estimated to be around 1200 K (Clark et al., 2003). At this temperature, potassium and graphitic carbon could be thermally ionized significantly due to the fact that they have low ionization potential of 4.34 and 8.5 eV, respectively (Shuler and Weber, 1954).

2.3.2. Chemi-ionization of flame species

Chemi-ionization is another possible mechanism by which significant ionization may occur in wildfire flames (Latham, 1999). In the process, dissociation reactions provide part of the energy required for ionization since there are exothermic and the rest is from the flame. After the combustion of vegetative matter, alkaline earth metal oxide and carbonates settle as ash. There is a high possibility that soon after their formation in the flame, they react with one of the main product, and carbon monoxide (CO), to produce electrons and carbon dioxide (CO_2) see Alkemade (1979). An example of the dissociation reaction is when an alkaline earth metal oxide such as calcium oxide (CaO) reacts with CO. The reaction may proceed in the following manner:

$$CaO + CO \Leftrightarrow Ca^{+} + e^{-} + CO_2. \quad (2)$$

During the plant matter combustion, freed potassium species thermally dissociate to atoms. However, not all thermally ionize; some dissociated potassium atoms may also react in the following manner to give electrons to the hot gaseous medium:

$$K + CO + O \Leftrightarrow K^{+} + e^{-} + CO_2. \quad (3)$$

Australian vegetation contain upto 1.1% chlorine on dry mass basis (Judd et al., 1996). In plant matter, chlorine exists in soluble form mostly attached to alkali atoms, e.g., as KCl (Jensen et al., 2000). After thermal decomposition of the alkali chloride in very hot wildfires, chlorine ions in the flame may also contribute to the ionization by reacting with hydrogen atoms, also present in the flame, to give electrons according to the following equation:

$$Cl^{-} + H \Leftrightarrow e^{-} + HCl. \quad (4)$$

Exited methyl radical CH^{*} is a known contributor to ionization in the hydrocarbon flames, e.g., in Sorokin et al. (2002) and Gaydon and Wolfhard (1978). CH radical reacts with oxygen atoms in the flame to produce CHO^{+}, a primary ion in hydrocarbon flames (Butler and Hayhurst, 1998) and electrons according to the following reaction equation:

$$CH^{*} + O \Leftrightarrow CHO^{+} + e^{-}. \quad (5)$$

2.3.3. Dominant ionization mechanism in grassfires

Most of the carbon atoms that exit in flames are in a coagulated form called soot. Soot is submicroscopic in size and has graphite structure (infinite large aggregate of carbon atoms) although smaller than the latter. The electrochemical characteristics of soot are different from both carbon and graphite. Ionization potential (ϕ_{ip}) increases from graphite ($\phi_w = 4.35$ eV) to carbon ($\phi_{ip} = 11.26$ eV), thus ϕ_{ip} decreases from a small to large carbon structure. Structurally, soot lies between carbon and graphite polymer, therefore it is reasonable to suggest that its ϕ_w should be between 4.35 and 11.26 eV. ϕ_w for soot has been experimentally determined to be 8.5 eV (Shuler and Weber, 1954). With ϕ_w almost twice that of potassium, the presence of potassium in flames is then the most effective source of thermal ionization in wildfires.

Temperature and concentration of species make chemi-ionization of flame particles less important than thermal ionization of potassium in the fire, e.g., potassium chloride (KCl) has high dissociation energy of 4.43 eV compared to other potassium species. Very hot grassfires are necessary for appreciable dissociation of KCl particles. Significant thermal decomposition of KCl has been observed to occur between 900 and 1100 °C (Ljung and Nordin, 1997). Besides, after the decomposition, the concentration of chloride ions (Cl^{-}) may be affected by the presence of AAEM cations such as Ca^{2+} and Na^{+}, which form metal chlorides with the ions. Therefore, the contribution of Eq. (4) to flame ionization is insignificant compared to thermal ionization of K species. Oxygen (O_2) has high dissociation energy (5.5 eV) compared to potassium species, therefore the availability of O atoms in Eqs. (3) and (5) is also temperature and species concentration dependent. In Eq. (2), CaO is formed at the hottest part of the flame and then precipitate to the ground while CO is usually formed in cooler parts of the fire, therefore very high intensity fires will promote the production of CaO and suppress the formation of CO. Generally the presence of

potassium seeding thermal ionization a dominant mechanism for electron production (Belcher and Sudden, 1950).

2.4. Radio wave attenuation by grassfires

At microscopic scale, electrons appear to be in random motion. However, at macroscopic scale electrons have a directed motion, a drift in the direction of the impressed electric field. If the applied electric field and the thermal energy are not high enough to deviate the energy distribution from Maxwellian as is the case with grassfires, then equation of motion for an average electron in the slightly ionized gaseous medium undergoing repetitive collisions is given as

$$m\ddot{x} + m\upsilon_{\text{eff}}\dot{x} = q_{\text{e}}\left[\vec{E} + \frac{\dot{x}}{c} \wedge \vec{B}\right], \tag{6}$$

where $\dot{x}$ and $\ddot{x}$ are the drift velocity and acceleration of an average electron; E and B are electric and magnetic field vectors; c, m and q_{e} are speed of light, mass and charge of an electron charge; and υ_{eff} is the effective momentum transfer collision frequency. The right-hand side of Eq. (6) is Lorentz electromagnetic force. The contribution of B in the Lorentz force is so small that it can be neglected. To solve equation for $\dot{x}$, E and $\dot{x}$ are assumed to vary as $\mathrm{e}^{\mathrm{i}\omega t}$ such that $E = E_0\mathrm{e}^{\mathrm{i}\omega t}$, and similarly for $\dot{x} = \dot{x}_0\mathrm{e}^{\mathrm{i}\omega t}$. We then have,

$$\dot{x} = \frac{q_{\text{e}}}{m(\upsilon_{\text{eff}} + \mathrm{i}\omega)}\vec{E}. \tag{7}$$

The following relation relates the drift velocity of an average electron to the current density (J); $J = N\dot{x}q_{\text{e}}$, where N is the electron density. Also $J = \sigma E$, this gives electric conductivity of the weakly ionized flame as

$$\sigma = \frac{Nq_{\text{e}}^2}{m(\upsilon_{\text{eff}} + \mathrm{i}\omega)} = \sigma_{\text{r}} + \mathrm{i}\sigma_{\text{i}}. \tag{8}$$

Eq. (8) is a complex function with real part:

$$\sigma_{\text{r}} = \frac{\varepsilon_0\omega_{\text{p}}^2\upsilon_{\text{eff}}}{(\upsilon_{\text{eff}}^2 + \omega^2)}. \tag{9}$$

And the imaginary part

$$\sigma_{\text{i}} = -\frac{\varepsilon_0\omega_{\text{p}}^2\omega}{(\upsilon_{\text{eff}}^2 + \omega^2)}, \tag{10}$$

where $\omega_{\text{p}}^2 = (Nq_{\text{e}}^2/m\varepsilon_0)$, ε_0 are the plasma collision frequency and free space permittivity.

Grassfire propagation constant is a measure of the rate of electromagnetic energy loss through the attenuation index and wave dispersion through the refractive index. Attenuation and refractive indices are dependent on the collision frequency and the electron density of a wildfire. These physical quantities can be determined from complex dielectric permittivity of the flame.

The dielectric permittivity for a wave in an ionized gas is given as

$$\varepsilon_{\text{r}} = 1 + \frac{\sigma_{\text{r}}}{\mathrm{i}\omega\varepsilon_0} + \frac{\sigma_{\text{i}}}{\omega\varepsilon_0}. \tag{11}$$

Substituting (9) and (10) into (11) gives

$$\varepsilon_{\text{r}} = \left[1 - \frac{\omega_{\text{p}}^2}{(\upsilon_{\text{eff}}^2 + \omega^2)}\right] - \mathrm{i}\left[\frac{\omega_{\text{p}}^2\upsilon_{\text{eff}}}{\omega(\omega^2 + \upsilon_{\text{eff}}^2)}\right]. \tag{12}$$

Propagation constant γ is, however, related to the dielectric permittivity constant by the following relation:

$$\gamma^2 = -\mu_0\varepsilon_0\omega^2\varepsilon_{\text{r}} \;\Leftrightarrow\; \gamma = \mathrm{i}\frac{\omega}{c}\sqrt{\varepsilon_{\text{r}}}. \tag{13}$$

Also γ can be written as

$$\gamma = \alpha_{\text{f}} + \mathrm{i}\beta_{\text{f}}, \tag{14}$$

where α_{f} and β_{f} are derived from Maxwell's equations for a wave $E = E_0\mathrm{e}^{-\mathrm{i}\gamma x}$ as

$$\alpha_{\text{f}} = \frac{\omega}{c}\left\{-\frac{1}{2}\left(1 - \frac{\omega_{\text{p}}^2}{\omega^2 + \upsilon_{\text{eff}}^2}\right) + \frac{1}{2}\left[\left(1 - \frac{\omega_{\text{p}}^2}{\omega^2 + \upsilon_{\text{eff}}^2}\right)^2 + \left(\frac{\omega_{\text{p}}^2}{\omega^2 + \upsilon_{\text{eff}}^2}\frac{\upsilon_{\text{eff}}}{\omega}\right)^2\right]^{1/2}\right\}^{1/2}, \tag{15}$$

$$\beta_{\text{f}} = \frac{\omega}{c}\left\{\frac{1}{2}\left(1 - \frac{\omega_{\text{p}}^2}{\omega^2 + \upsilon_{\text{eff}}^2}\right) + \frac{1}{2}\left[\left(1 - \frac{\omega_{\text{p}}^2}{\omega^2 + \upsilon_{\text{eff}}^2}\right)^2 + \left(\frac{\omega_{\text{p}}^2}{\omega^2 + \upsilon_{\text{eff}}^2}\frac{\upsilon_{\text{eff}}}{\omega}\right)^2\right]^{1/2}\right\}^{1/2}. \tag{16}$$

Atmospheric plasmas are highly collisional (Laroussi and Roth, 1994), so we may assume that flames are weakly ionized, therefore at HF–VHF radio wave frequencies $\upsilon_{\text{eff}} > \omega \gg \omega_{\text{p}}$. Eqs. (15) and (16) reduce to

$$\alpha_{\text{f}} \cong \frac{\upsilon_{\text{eff}}}{2c}\left[\frac{\omega_{\text{p}}^2}{(\omega^2 + \upsilon_{\text{eff}}^2)}\right] \tag{17}$$

and

$$\beta_f \cong \frac{\omega}{c}\left[1+\frac{\omega_p^4}{8(\omega^2+\upsilon_{eff}^2)^2}\frac{\upsilon_{eff}^2}{\omega^2}\right]. \quad (18)$$

3. Partition functions

3.1. Single atoms

Internal partition functions of particles can be calculated from the relations given in Joint Army, Navy, and Air Force (JANAF) tables (Chase et al., 1985). For single atoms and ions, Chase et al. (1985) gave the internal partition function of single atoms and ions as

$$Q_{int}(T)=\sum_n \omega_n \exp\left(\frac{-E_n}{kT}\right), \quad (19)$$

where E_n is energy at excited level and ω_n is statistical weight at level n.

3.2. Diatomic molecules and ions

Using a rigid-rotor model (e.g., in Andre, 1995), the internal partition function of ideal diatomic molecules is given by Maouhoub et al. (1999) as

$$Q_{int}(T)=\sum_n \frac{kT}{hcB_e\sigma}\frac{\omega_n \exp(-E_n/kT)}{[1-\exp(-hc\omega_e/kT)]}, \quad (20)$$

where B_e and ω_e are rotational and vibration constants; σ is symmetry number; and c is speed of light.

3.3. Polyatomic molecules and ions

Gibbs free energy is used to calculate the internal partition energy of these particles. Chase et al. (1995) relate Gibbs free energy (G^0) to the total partition function (Q_t) of a particle by

$$-[G^0(T)-H^0(0\ \mathrm{K})]/RT=\ln Q_t, \quad (21)$$

where H^0 is enthalpy of formation of a particle and R is gas constant.

Total partition function of a particle (Q_t) is a product of internal and translational partition functions i.e.

$$Q_t = Q_{int}.Q_{tr}. \quad (22)$$

From Eq. (22), the internal partition function of a polyatomic particle is given by Maczek (1998) as

$$Q_{int}=\frac{Q_t}{[2\pi kT/h^2]^{2/3}kT/P}, \quad (23)$$

where P is the total plasma pressure, given by Dalton's Law of partial pressures of individual gases in plume as

$$P=\sum_{i=1}^{\alpha} N_i kT, \quad (24)$$

where N_i is species number concentration of a plume gas.

4. Numerical experiment

4.1. Physical dimensions and behaviour of the simulated grassfires

Propagation characteristics of radio signals through a moderate to high intensity grassfires are simulated in the numerical experiment. Most of these fires occur in Sorghum spp. grasslands or in open woodland where the grasses are dominant understorey vegetation. During the season, intensity of the fires could be up to 18 MW m^{-1}(Williams et al., 2003). The fire simulated in here has similar physical dimensions and characteristics to those simulated by Clark et al. (2003). The dimensions of the grassfire used in the simulation are given in Fig. 1.

The depths of the simulated line grassfires increase with maximum temperature at the interface. Depths of the fires considered are as shown in Table 1. Volatile flux and vertical velocity are taken to be 0.1 kg m^{-2} s^{-1}and 5 m s^{-1}, respectively. These values were measured in experimental grassfires in Northern Australia (see Clark et al., 2003). It is assumed that the combustion is near complete with efficiency of 98%. Up to 20% of the volatilized alkalis are available for thermal ionization (Vodacek et al., 2002).

4.2. Temperature of the grassfire flame

The grassfires considered for simulation are assumed to have reached a state of quasi-equilibrium, hence spread at a constant rate in the grass fuel. Maximum temperatures at the *fuel–flame* interface of the simulation range from 900 to 1150 K. The temperature decreases exponentially with height from the interface. Fig. 2 shows the

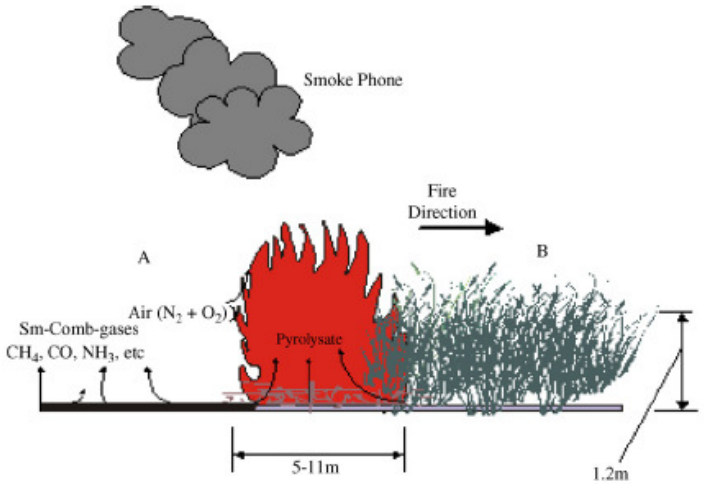

Fig. 1. Physical dimensions of the grassfire considered in the simulation experiment.

Table 1
Fire depth at fuel–fire interface for maximum temperatures from 900 to 1150 K

Maximum temperature at *fue–fire* interface (K)	900	1000	1100	1150
Fire depth (m)	5.44	6.80	8.72	10.43

temperature decrease for a typical grassfire with *fuel–flame* interface, which is at 1200 K. The exponential decrease is such that at 1.5 m above ground level temperature is 998 K. Across the grassfire depth, temperature assumes Rayleigh profile (see Fig. 3) and it varies as (Oliveira et al., 2002):

$$T_{\mathrm{fl}} = T_{\mathrm{amb}} + \frac{\alpha\beta}{\zeta'}\exp\left\{-\left(\frac{\beta}{\zeta'}\right)^2\right\}, \tag{25}$$

where α and β are empirically determined constants, ζ' is distance from to arbitrary origin of the curve. Ignition temperature is approximated to be approximately 300 °C (e.g., in Morandini et al., 2002) and it is used in the experiment to define flame depth of the grassfires.

4.2.1. Step function approximation of temperature at fuel–fire interface

To make predictions of ionization density in the grassfire, a state of thermal equilibrium is assumed.

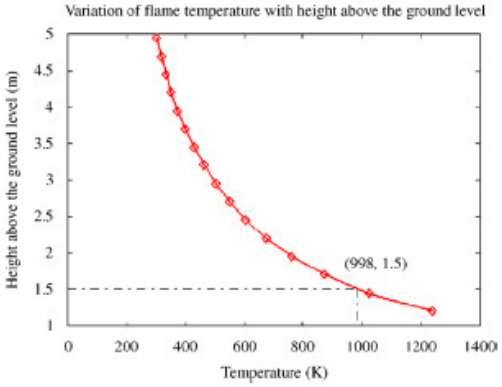

Fig. 2. Typical variation of temperature with height above ground of the grassfire plume.

Under thermal equilibrium, the grassfire flame depth at the interface is divided into elementary volumes (mini-slabs) of equal thickness (dw), which are a certain fraction of the flame depth. The mini-slabs assume a statistical average temperature (T) which is defined by a Rayleigh distribution. This results in a step function approximation of Rayleigh profile of temperature across the fire depth at the interface. The step function is illustrated in Fig. 4. The numerical simulation considers line grassfires with semi-infinite width. Temperature along the width is assumed to be invariant at any height above

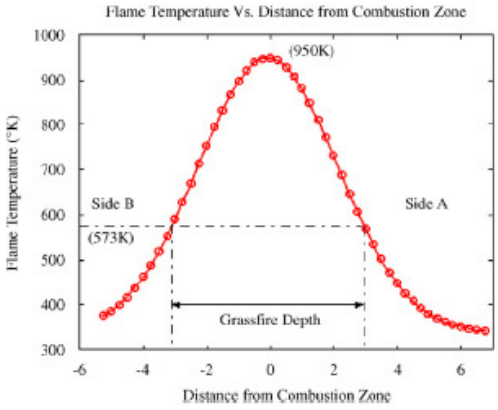

Fig. 3. Temperature variation across the grassfire depth at fuel–fire interface for a maximum flame temperature of 950 K.

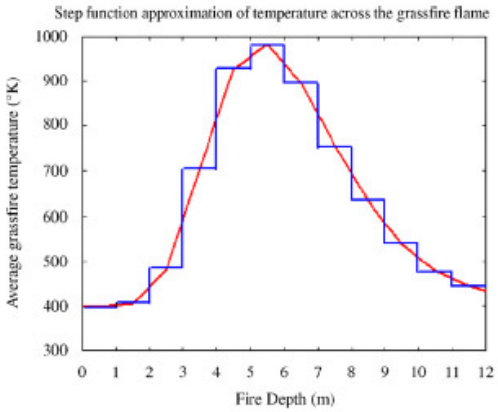

Fig. 4. Step function approximation of temperature across grassfire flame depth.

the grass canopy. It only varies across the fire depth as it is shown in Fig. 3.

4.3. The number of alkali atoms in a mini-slab

Let the mass of potassium drawn with the volatile flux into the grassfire flame in a unit time be M_p and its percentage in volatile flux be P_k. Let also volatile flux and vertical velocity be given as V_f and V_v, respectively, as is it is shown in Fig. 5. The mass of potassium in the grassfire flame per unit volume in a unit time is

$$M_p = \frac{P_k.V_f}{V_v}\ \text{kg}. \tag{26}$$

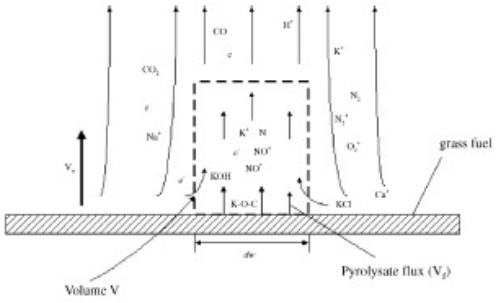

Fig. 5. Potassium species swept into a unit volume of a grassfire flame.

The number of potassium atoms (η) swept into a unit volume in a unit time is

$$\eta = \frac{M_p.N_a}{0.03903}\ \text{atoms}, \tag{27}$$

where N_a is avogadro number.

4.4. Dissociation of flame particles in a mini-slab

Volatiles are released from the vegetation's organic matrix and swept by convective currents into the combustion zone of flames (see Fig. 5). In the mini-slabs, alkali atoms released from charcoal (Okuno et al., 2005) are directly thermally ionized at the local kinetic temperature into electrons and alkali ions. Potassium and sodium have ionization potential of 4.34 and 5.14 eV, respectively. Alkali molecules such as KCO_3 (g), KOH (g), etc. are thermally dissociated first and then ionized thereafter. Dissociation energy of potassium salts are low, they range from as low as 0.75 eV to about 4.51 eV (KCl). KOH has dissociation energy of about 3.51 eV. The number concentrations of singly ionized and neutral particles in the grassfire plume may also depend on disassociation of the volatilized diatomic and polyatomic molecules according to the following relation:

$$\text{AB(g)} \Leftrightarrow \text{A(g)} + \text{B(g)}, \tag{28}$$

where AB (g) is pyrolysate parent molecule and A (g), B (g) are daughter particles.

If thermal equilibrium is assumed, the number concentration of dissociated particles can be determined by using Guldberg–Waage law. Koalaga

(2001) gave the law as

$$\frac{N_A N_B}{N_{AB}} = \frac{Q_{Aint} Q_{Bint}}{Q_{ABint}} \left(\frac{2\pi k T}{h^2}\right)^{3/2} \left(\frac{m_A m_B}{m_{AB}}\right)^{3/2} \times \exp\left(\frac{-E_d}{kT}\right), \quad (29)$$

where N_A, N_B and N_{AB} are number concentration of A, B and AB, respectively; Q_{Aint}, Q_{Bint} and Q_{ABint} are internal partition function of A (g), B (g) and AB (g); E_d is dissociation energy; k is Boltzmann constant; h is Planck constant; m_A, m_B, m_{AB} are masses of particles; and T is thermodynamic temperature.

Exothermic chemical reactions that occur in the combustion zone render it hot enough to cause thermal disintegration of some pyrolysed species including the AAEM based salts into atoms and their associated species. Alkali metal salts in the pyrolysate are more likely to be thermally decomposed due to low dissociation energies; for an example potassium hydroxide and sodium chloride have dissociation energies 3.51 and 4.24 eV, respectively. The dissociation energy could be much less for complex organic salts of alkali such as *malate* or oxalate.

4.5. Ionization in mini-slabs

Electron density in mini-slabs is calculated from the Saha–Eggert equation (Eq. (33)). It is assumed that the most significant contribution to ionization is from light gases and hydrogen radical displaced potassium atoms (K) from the charcoal matrix. Potassium atoms released from charcoal matrix are from K–O–C) (Okuno et al., 2005). Dissociated potassium atoms from KCl (g) and KOH (g) are also considered. KCl (g) is stable at temperatures below 1000 K; however, it dissociates significantly at temperatures around 1400 K.

Dissociated atoms such as A (in Eq. (28)) are electronically excited by the thermal energy in the reaction zone making them very unstable, thus giving atoms in the state A^*. On collision with other flame species (S) the atoms they give out their outer shell electron to produce singly ionized particles (A^+). Reaction equation (30) gives an account of ionization of excited atoms on collision with species S (Butler and Hayhurst, 1998):

$$S(g) + A^*(g) + S(g) \Leftrightarrow A^+(g) + e^-(g) + S(g). \quad (30)$$

However, the overall equation for Eq. (30) is

$$A(g) \Leftrightarrow A^+(g) + e^-(g). \quad (31)$$

Similarly, an equation that represents the ionization of diatomic species such NO is given by Koalaga (2001) as

$$AB(g) \Leftrightarrow AB^+(g) + e^-(g). \quad (32)$$

To quantify the approximate amount of ionization due to thermal ionization and the composition of the flame mini-slab, the application of Saha and Guldberg–Waage equations is sufficient as long as the flame mini-slab is assumed to be in LTE (Koalaga, 2001). Chen and Han (1999) gave the Saha equation as

$$\frac{N_{m^+} N_e}{N_m} = \frac{2 Q_{m^+\,int}}{Q_{m\,int}} \left(\frac{2.\pi.m.kT}{h^2}\right)^{3/2} \exp\left(\frac{-(E_i)}{kT}\right), \quad (33)$$

where N_{m^+} N_e and N_m are number concentration of singly ionized particles, electrons and neutral particles, respectively; $Q_{m\,int}$ and $Q_{m^+\,int}$ are internal partition function of particles; E_i, and m are ionization energy and mass of an electron. The rest of the variables are as defined earlier. Eq. (33) is the ionization equilibrium constant (K_1) in a mini-slab. Electron density (N_e) due to thermal ionization of K atoms is related the ionization equilibrium constant and the total number of ionized K particles (N_p) in the flames as (Frost, 1961):

$$N_e = (K_1 N_p)^{1/2} \left[\left(1 + \frac{K_1}{4N_p}\right)^{1/2} - \left(\frac{K_1}{4N_p}\right)^{1/2}\right]. \quad (34)$$

The total number of ionized K particles (N_p) in a mini-slab is related to the potassium atoms in the flame by the equation:

$$N_p = \frac{7.335 \times 10^{27} \eta}{T}\ m^{-3}, \quad (35)$$

where η is the number density of K atoms into the combustion zone of a mini-slab.

Using Eqs. (34) and (35), which assumes thermal equilibrium, ionization in flames has been predicted with a fair amount of accuracy because electron-scavenging radicals such as hydroxyl (OH) are taken into account (Frost, 1961). In the prediction of ionization density in a grassfire, we follow these authors and use LTE assumption for a *first approximation* of ionization density.

The quasi-neutrality condition must hold in a mini-slab. Thus, the sum of all charges in the plasma system must be equal to zero. This condition is given as

$$\sum_{i=1}^{\alpha} n_i^+ = N_e. \tag{36}$$

4.5.1. An example of calculation of electron density in a mini-slab

Consider a wildfire to burn in a grass which naturally contains an average potassium content of 2.0%. The wildfire is considered to be of near complete (99%) combustion efficiency. During the combustion, 20% of the inherent K is emitted together with the volatiles in the combustion zone of average temperature of 1100 K (e.g., in Vodacek et al., 2002). Therefore, overall percentage of potassium in the volatiles (P_k) is 0.04. The K in volatiles is emitted as K atoms from a displacement reaction of K–O–C with H^+ (as in Section 2.3.1). Using Eq. (26), mass of K per unit volume in a unit time (M_p) is 8.00×10^{-5} kg. The number of potassium atoms (η) is calculated from Eq. (27) as 1.234×10^{21} atoms. The number of ionized potassium particles (N_p) is calculated from Eq. (35). Partition functions for potassium ions and atoms at 1100 K as calculated from Eqs. (21) and (19), respectively, are 1 and 2. The partition function of an electron is 2. The ionization energy for potassium is 4.34 eV. Using the partition functions and ionization energy for potassium, K_I is calculated from Eq. (33) and ultimately electron density (N_e) is determined from Eq. (34) as $4.36 \times 10^{16}\,m^{-3}$.

Electron densities for grassfires with maximum flame temperatures between 950 and 1150 are plotted using Eq. (34) in Fig. 6. The electron densities are up to $5.2 \times 10^{16}\,m^{-3}$ for flame maximum temperature of 1150 K and 2% plant potassium content. The electron densities so obtained are used to calculate relative dielectric permittivity of mini-slabs used in the thermal equilibrium model as per Eq. (12).

4.6. Collision frequency in the dielectric mini-slabs

The collision frequency in the mini-slabs depends on their average temperature. It is calculated from the expression:

$$\upsilon_{eff} = N_n \sigma_c \sqrt{K_B T m}. \tag{37}$$

For temperatures near 1000 K, $\upsilon_{eff} = 10^{11} P$, where P is pressure in atmospheres.

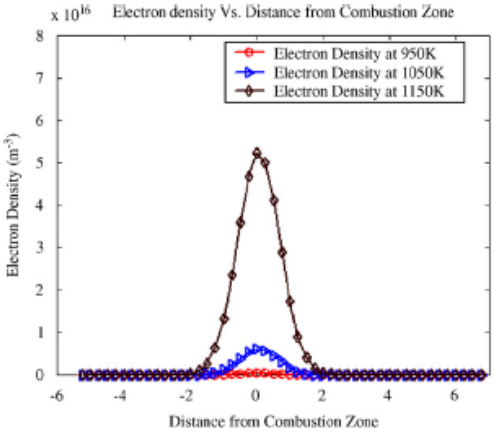

Fig. 6. Variation of electron density at different temperatures with distance from combustion zone.

4.7. Grassfire flame as a composite of dielectric mini-slabs

The fuel–flame interface is considered a composite of mini-slabs with varying electron density and dielectric permittivity as governed by step-function approximation of temperature. The physical properties of the flame are calculated from average temperature and electron density, respectively. Fig. 7 shows the variation of electron density with fire depth of a grassfire at a temperature of 940 K. In the experiment mini-slabs of 0.25 m are used to the model the radio wave propagation characteristic in the grassfires.

4.8. Transmission and reflection power fractions

For propagation of radio waves at normal incident to the line grassfire width, the reflection coefficient equation at $(m+1)$th mini-slab of the composite in Fig. 7 is given by Laroussi and Roth (1994) as

$$R_{m+1} = \frac{E_r}{E_0} = \frac{(\varepsilon_{m+1}/\varepsilon_m) - (\varepsilon_{m+1}/\varepsilon_m)^{1/2}}{(\varepsilon_{m+1}/\varepsilon_m) + (\varepsilon_{m+1}/\varepsilon_m)^{1/2}}. \tag{38}$$

Total transmitted power fraction (P_{tf}) for the whole slab arrangement is given by Tang et al. (2003) as

$$P_{tf} = \prod_{l=1}^{sn}[(1 - |R_{m+1}|^2)][\exp(-2\alpha_f(i)d)]]. \tag{39}$$

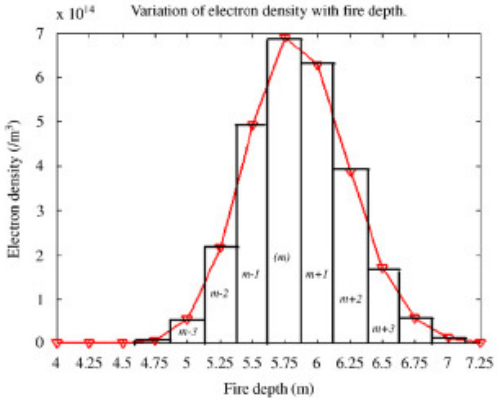

Fig. 7. Variation of electron density, temperature with fire depth.

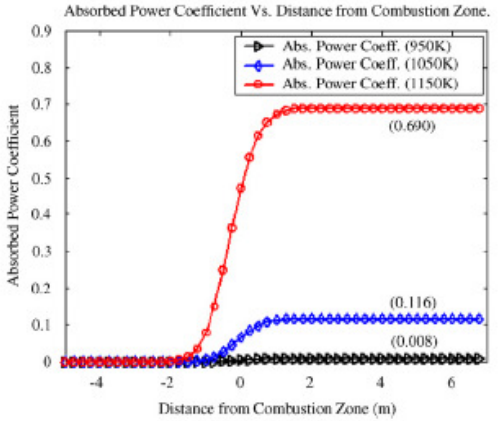

Fig. 8. Variation of total absorbed power fraction with distance from the combustion zone.

Total reflected power fraction for the composite is also given by Tang et al. (2003) as

$$P_{rf} = \left\{ R_1^2 + \sum_{i=2}^{sn} \left[(R_i)^2 \prod_{i=1}^{sn-1} ((1 - |R_i|^2) \times (\exp[-4\alpha_f(i)d]) \right] \right\}. \quad (40)$$

5. Numerical results and discussions

5.1. Transmitted and absorbed power fractions

The transmitted and absorbed power fraction of radio waves in grassfire flames at maximum combustion zone temperatures of 950–1150 K were simulated for when up to 20% of the pyrolysates are ionizable potassium species. Potassium content in vegetation was taken to be 2% on dry weight basis. Simulations show that total reflected power of radio waves from flames of physical characteristics described in Table 1 is generally negligible; hence graphs of variation of total reflected power with fire depth are not shown. Transmitted power fractions were observed to be generally affected significantly within flame radius of 2 m from the combustion zone. This decreased markedly with the increase in maximum combustion zone temperature. At maximum combustion zone temperature of 1150 K the power of transmitted radio waves decreased to 31% of the incident. At 950 K it decreased to 99% of the incident power. Power of radio waves which propagate through a grassfire with maximum combustion zone temperature of 1050 K is 88% of the incident. Fig. 8 shows the transmitted power fractions of the waves through the grassfires.

The reduction in the transmitted power of radio wave through grassfire was mainly brought about by collisional damping of the waves in the ionized grassfire flames since reflected power was negligible. The grassfire medium is highly collisional because it is at atmospheric pressure. Maximum combustion zone electron densities in the grassfire flames ranged from 10^{14} to $10^{17}\,m^{-3}$.

Absorbed power fractions were observed to increase with the increase in maximum combustion zone temperature. At 950 K, absorbed power fraction was noted to be 0.8% of that incident while at 1150 K it was 69% of the incident. Fig. 9 shows the variation of absorbed power fraction with distance from the combustion zone. Most of the absorption occurred within a radius of 2 m from the combustion zone.

5.2. Specific attenuation and phase change

Specific attenuation of radio waves at a fuel–fire interface has been observed to increase with the increase in both maximum combustion zone temperature and percentage of potassium in vegetation. The thermal equilibrium model predicts specific attenuation of up $0.49\,dB\,m^{-1}$ at the maximum

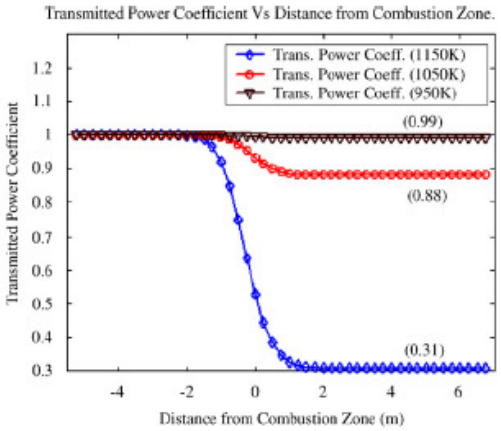

Fig. 9. Variation of transmitted power fraction with distance from the combustion zone.

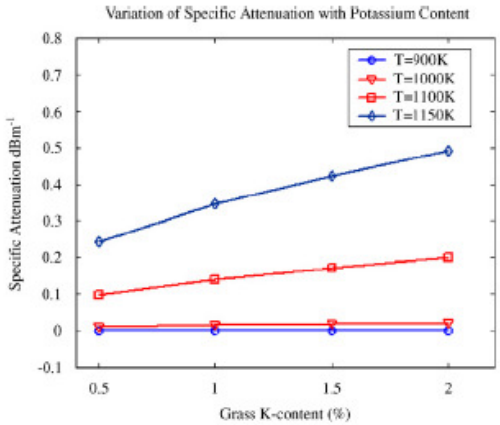

Fig. 10. Variation of specific attenuation with grass potassium content.

temperature of 1150 K and 2% potassium content in grass. This maximum temperature considered in the simulations is common in grassfires of Australian tropical grassland savannas, where *Sorghum* spp. predominate (Clark et al., 1996). On average, potassium content in *Sorghum* spp. is 1.06% (Cook and Andrew, 1991).

At the average potassium content, the thermal equilibrium model predicts specific attenuation which ranges from 0.001 to 0.35 dB m^{-1} for the combustion temperatures 900–1150 K. At 2% potassium content in grass the thermal equilibrium model predicts 0.001–0.42 dB m^{-1} for the maximum combustion zone temperatures of 900–1150 K. Propagation measurements carried out by the authors in a prescribed grassfire in open woodland vegetation gave a specific attenuation of 0.025 dB m^{-1} for spear grass (*Heteropogon Contortus*) with potassium content of about 1.29% on dry weight basis (Mphale, 2005). Maximum flame temperature for the grassfire was about 900 K.

Specific phase changes vary in a similar way as the specific attenuation. The model predicts 152° m^{-1} specific phase change at the maximum combustion temperature of 1150 K. This, however, decreases to a value of 38° m^{-1} at potassium content of 0.5%. Maximum combustion temperature of 1100 K yielded specific phase change ranges from 6 to 22° m^{-1} for potassium content of 0.5–2.0% in grass. The specific phase change varied from 0.0002 to 0.23° m^{-1} for the temperature range of 900–1000 K (Figs. 10, 11).

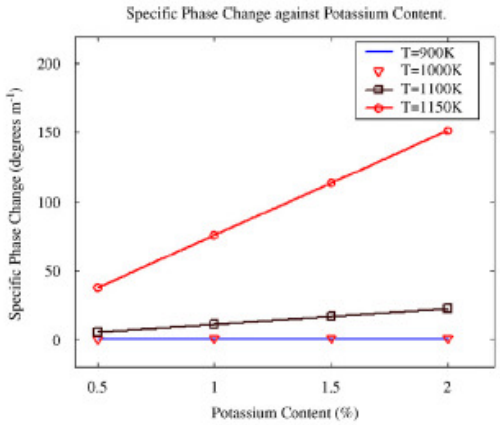

Fig. 11. Variation of specific phase change with grass potassium content.

Experimentally, flame radio wave attenuation and phase change can be determined by line-of-sight (LOS) propagation measurements, e.g. in Koretzsky and Kuo (1998), Belcher et al. (1950) and Shuler et al. (1954). Attenuation per unit path length of 10 GHz waves in very hot alkali seeded coal-air flames was observed to be around 1 dB cm^{-1} (Belcher et al., 1950). Koretzsky measured 25 dB of X-band loss in plasma torch flames over a propagation path of 6 cm. A vector network analyser could also be used to determine the parameters. Temperature of a flame could be experimentally determined by wiring a data logger

connected thermocouples to measure temperature at any point of the flame. For flames in cylindrical cavities, temperature assumes Gaussian profile. It is highest at the centre and gradually decreases to the cavity wall, e.g., Dupuy et al. (2003).

6. Conclusions

The contribution of alkali species to the ionization in wildfires cannot be ignored more especially at flame temperatures more than a 1000 K. The thermal equilibrium model predicts electron densities in the range of 10^{14}–$10^{17}\,m^{-3}$ due to alkali species in the flame. The thermal equilibrium model has an advantage of taking into account electron loss processes in flame such as scavenging by hydroxide radical. Assuming Maxwellian velocity distribution and at collision frequency of about $10^{11}\,s^{-1}$, total transmission power fraction is predicted to fall to 99.2% of the incident at 950 K while at 1150 K, the total transmitted power fell to 31% of the incident power. This occurred at grass potassium content of 2% on dry weight basis. Most of the lost energy in the grassfire flames is due to absorption. A negligible amount of radio wave energy is reflected.

Grassfire with temperatures ranging from 900 to 1150 K are predicted by the thermal equilibrium model to have specific attenuation of 0.001–$0.49\,dB\,m^{-1}$. At low potassium content of 0.5% at the same temperature range, specific attenuation ranges from 0.0007 to $0.24\,dB\,m^{-1}$. The specific attenuation increased with the increase in potassium content in grass and temperature of the flame. The contribution of potassium in the flame to radio wave energy loss at temperatures less than 1000 K is not significant. Specific phase changes for grassfire with the temperature range of 900–1150 K were $0.001–152^{\circ}\,m^{-1}$ at 2% potassium content in grass. The specific phase change decreased with the decrease in potassium content. At potassium content of 0.5% the specific phase change was observed to be $0.0002–38^{\circ}\,m^{-1}$.

Acknowledgement

We would like gratefully to acknowledge Staff Development Office of the University of Botswana for the financial support for this work. The work was partly supported by Emergency Management Australia under project no. 60/2001.

References

Alkemade, M.A., 1979. Fundamentals of Analytical Flame Spectroscopy. Hilger, Bristol.

Andre, P., 1995. IEEE Transactions on Plasma Science 23, 453.

Belcher, H., Sudden, T.M., 1950. Proceedings of the Royal Society A 202, 17.

Brown, A.A., Davis, K.P., 1973. Forest Fire: Control and Use. McGraw Hill, New York.

Butler, C.J., Hayhurst, A.N., 1998. Kinetics of gas-phase ionization of an alkali metal, A, by the electron and proton transfer reactions: $A+H_3O^+ \rightarrow A+.H_2O+H$; $AOH+AOH_2++H_2O$ in fuel-rich flames at 1800–2250 K. Journal of the Chemical Society Faraday Transactions 98, 2729–2734.

Chase, M.W., Davies, C.A., Downey, J.R., Frurip, D.J., McDonald, R.A., Sqverud, A.N., 1985. Journal of Physical Chemistry Reference Data 14, 1.

Chen, X., Han, P., 1999. Journal of Physics D: Applied Physics 32, 1711.

Cheney, N.P., Gould, J.S., Catchpole, W.R., 1993. The influence of fuel, weather and fire shape variation in fire spread in grassland. International Journal of Wildland Fire 3, 31–44.

Clark, T.L., Griffiths, M., Reeder, M.J., Latham, D., 2003. Numerical simulations of grassland fires in the Northern Territory, Australia: a new subgrid-scale fire parameterization. Journal of Geophysical Research 108 D18(4589), ACL 14-1–14-15.

Cook, G.D., Andrew, M.H., 1991. The nutrient capital of indigenous Sorghum species and other understorey components of Savannas in north-western Australia. Australian Journal of Ecology 16, 375–384.

Davidson, K.O., Korsgren, J.G., Pettersson, J.B.C., Jaglid, U., 2002. Fuel 81, 137–142.

Dupuy, J.L., Marechal, J., Morvan, D., 2003. Fires from a cylindrical forest fuel burner: combustion dynamics and flame properties. Combustion and Flame 135, 65–76.

Engstrom, J.D., Butler, J.K., Baxter, L.L., Fletcher, T.H., Weise, D.R., 2004. Ignition behavior of live Chaparral leaves. Combustion Science and Technology 176, 1577–1591.

Frost, L.S., 1961. Conductivity of seeded atmospheric pressure plasmas. Journal of Applied Physics 32, 2029–2036.

Foster, T., 1976. Bushfire: History, Prevention and Control. A. H. and A.W. Reed Pty Ltd, Sydney.

Gaydon, A.G., Wolfhard, H.G., 1978. Flames: Their Structure, Radiation and Temperature, fourth ed. Chapman & Hall, London.

Jensen, A.P., Frandsen, F.J., Dam-Johansen, K., Sander, B., 2000. Experimental investigation of the transformation and release to gas phase of potassium and chlorine during straw pyrolysis conditions. Energy and Fuels 11, 1026–1032.

Judd, T.S., Attiwill, P.M., Adams, M.A., 1996. Nutrient concentrations in eucalyptus: a synthesis in relation to difference between taxa, sites and components. In: Attiwill, P.M., Adams, M.A. (Eds.), Nutrition of Eucalypts. CSIRO Publishing, Melbourne, pp. 123–153.

Koalaga, Z., 2001. Determination of equilibrium composition of CxHyOzNt plasmas out of thermodynamic equilibrium. European Physics Journal D 17, 235–247.

Koretzsky, E., Kuo, S.P., 1998. Characterization of atmospheric pressure plasma generated by a plasma torch array. Physics of Plasmas 5 (10), 3774–3780.

Korsgren, J.G., Hald, P., Davidson, K.O., Pettersson, J.B.C., 1999. Characterisation of alkali metal emission from fuel and samples collected from fluidized bed gasification. In: Proceedings of the 15th International Conference on Fluidized Bed Combustion. ASME, Georgia.

Laroussi, M., Roth, J.R., 1994. Numerical calculation of the reflection, absorption, and transmission of microwave by a nonuniform plasma slab. IEEE Transaction on Plasma Science 21 (4), 366–372.

Latham, D., 1999. Space charge generated by wind tunnel fires. Atmospheric Research 51, 267–278.

Ljung, A., Nordin, A., 1997. Theoretical feasibility for ecological biomass ash recirculation: chemical equilibrium behavior of nutrients elements and heavy metals during combustion. Environmental Science and Technology 31, 2499–2504.

Maczek, A., 1998. Statistical Thermodynamics. Oxford Univeristy Press, Oxford.

Maouhoub, E., Coitout, H., Parizet, M.J., 1999. Excitation temperature measurements in an Argon—CO_2 thermal plasma. IEEE Transaction on Plasma Science 27 (5), 1469.

Maser, P., Gierth, M., Schroeder, J.I., 2002. Molecular mechanisms of potassium and sodium uptake in plants. Plant and soil 247, 43–54.

Morandini, F., Santoni, P.A., Balbi, J.H., Ventura, JM., Mendes-Lopes, J.M., 2002. A two-dimensional model of fire spread across a fuel bed including wind combined slope conditions. International Journal of Wildland Fire 11, 53–64.

Mphale, K.M., 2005. Radio wave propagation measurements and prediction in bushfires. Ph.D. Thesis, James Cook University, Australia.

Nussbaumer, T., 2003. Combustion and co-combustion of biomass: fundamentals, technologies and primary measures for emission reduction. Energy and Fuels 17, 1510–1521.

Obernbeger, I., Biedermann, F., Widmann, W., Riedl, R., 1997. Concentration of inorganic elements in biomass fuels and recovery in different ash fractions. Biomass and Bioenergy 12 (3), 211–224.

Okuno, T., Sonoyama, N., Hayashi, J., Li, C., Sathe, C., Chiba, T., 2005. Primary release of alkali and alkaline earth metallic species during pyrolysis of pulverized biomass. Energy and Fuels 19, 2164–2171.

Oliveira, L.A., Veigas, D.X., Vareli, V., Raimudo, A.M., 2002. On the soil thermal effect under the surface fire conditions. In: Proceedings of the Second International Conference on Forest Fire Research Coimbra, vol. III, D03, pp. 833–847.

Olsson, J.G., Jaglid, U., Pettersson, J.B.C., Hald, P., 1997. Energy and Fuel 11, 779–784.

Radojevic, M., 2003. Chemistry of forest fires and regional haze with emphasis on southeast Asia. Pure and Applied Geophysics 12, 157–187.

Raison, R.J., Khaina, P.K., Woods, P., 1985. Mechanisms of element transfer to the atmosphere during vegetation burning. Canadian Journal of Forest Research 15, 132–140.

Shuler, K.E., Weber, J., 1954. A microwave investigation of the ionization of hydrogen-oxygen and acetylene-oxygen flames. Journal of Chemical Physics 22, 491–502.

Sorokin, A., Vancassel, X., Mirabel, P., 2002. Emission of ions and charged soot particle by aircraft engines. Atmospheric Chemistry and Physics Discussions 2, 2045–2074.

Tang, D.L., Sun, A.P., Qiu, X.M., Chu, P., 2003. Interaction of electromagnetic waves with a magnetized nonuniform plasma slab. IEEE Transactions on Plasma Science 31 (3), 405–410.

Vodacek, A., Kremens, R.L., Fordham, S.C., VanGorden, S.C., Luisi, D., Schott, J.R., Latham, D.J., 2002. Remote optical detection of biomass burning using potassium emission signature. International Journal of Remote Sensing 23, 2721–2726.

Westberg, H.M., Bystrom, M., Lecker, B., 2003. Distribution of potassium, chlorine and sulphur between solid and vapour phases during combustion of wood and coal. Energy and Fuels 17, 18–28.

Williams, D.W., Adams, J.S., Batten, J.J., Whitty, G.F., Richardson, G.T., 1970. Operation euroka: an Australian mass fire experiment. Report 386, Maribyrnor, Victoria, Australia, Defense Standards Laboratory.

Williams, R.J., Cook, G.D., Gill, A.M., Moore, P.H.R., 1999. Fire regimes, fire intensity and tree survival in a tropical savanna in northern Australia. Australian Journal of Ecology 24, 50–59.

Williams, R.P., Congdon, R.A., Grice, A.C., Clarke, P.J., 2003. Effect of fire regime on plant abundance in tropical eucalypt savanna og north-eastern Australia. Austral Ecology 28, 327–338.